Influence of mean stress and PWR environment on the fatigue behavior of a 304L austenitic stainless steel

Ziling Peng, Gilbert Hénaff, Jean-Christophe Le Roux, Romain Verlet

Fatigue Crack Initiation and Propagation

4.1. Introduction

The resistance of metal alloys to fatigue can be classified into four major regimes: low-cycle fatigue (or short life), limited resistance (between 10^5 and 10^6 cycles), high-cycle fatigue (between 10^6 and 10^7 cycles) and gigacycle (more than 10^7 cycles). This chapter introduces the basic concepts of cyclic mechanical behavior, crack initiation and propagation in these different regimes.

4.2. Cyclic mechanical behavior, plastic fatigue

4.2.1. *Plastic or low-cycle fatigue tests*

Low-cycle fatigue is the regime associated with a load amplitude high enough to cause the fracture of a part after a limited number of cycles (typically less than 10^5 cycles). This is also plastic fatigue because a significant macroscopic plastic strain occurs with each cycle applied.

In order to analyze the mechanisms which cause low-cycle fatigue fractures, and to predict the associated life, it is necessary to carry out tests specifically developed to control the amplitude of the stress or strain applied. Thus, low-cycle fatigue tests are preferably carried out with controlled *plastic* strain amplitude, because the level of plastic strain evolves over time in metallic materials for a *total* deformation amplitude applied. The [ISO 17] standard which determines how these tests are performed, takes into account the possibility of these tests being carried out on all

Chapter written by Véronique DOQUET, Gilbert HÉNAFF, Thierry PALIN-LUC and Marion RISBET.

types of test specimens (flat, cylindrical, etc.), in the presence of a mean stress (for example, repeated fatigue[1], R > 0) or in the absence of mean stress (symmetrical alternating fatigue, R = –1). Low-cycle fatigue behavior tests are most commonly carried out under tension-compression (R = –1), with a weak effect of the load ratio in the low-cycle fatigue domain. The test is controlled by an extensometer to ensure constant plastic strain amplitude throughout the test.

The techniques used to detect the damage depend on the purpose of the test: the criterion for macroscopic damage (cracking of the test specimen or sudden drop of the load) in order to study a cyclic behavior model, or more accurate crack detection techniques if interested in the microscopic mechanisms at the origin of this type of fatigue. The observation of microcracks can be done with interrupted tests (removal of the specimen during the test and microscopic observation); however, the use of non-destructive testing techniques makes these observations less tedious. Some techniques have been widely used (electrical monitoring), while more recent ones are undergoing an important development (acoustic emission monitoring, detection of superficial cracks by *in-situ* observations, digital images correlation, X-ray phase contrast tomography [HER 11], etc.).

4.2.2. *Cyclic mechanical behavior*

The analysis of the hysteresis loop recorded during the test enables the characterization of the cyclic mechanical behavior of the material, which can vary depending on the nature of the alloy. For strain-controlled tests, the cyclic hardening (or softening) corresponds to an increase (or respectively decrease) of the stress amplitude (Figure 4.1(a)). This phase of transient accommodation often ends in a stabilization phase, where the hysteresis loop no longer evolves.

4.2.2.1. *Cyclic hardening and dislocation structures*

The cyclic hardening curves (saturation stress vs. strain amplitude, Figure 4.2(a)) enable establishing hardening laws which are generally different from the hardening laws in monotonic tension. A more detailed analysis of the hysteresis loops (Figure 4.1(b)) makes it possible to experimentally evaluate the kinematic and isotropic components of hardening, which can be described with adapted hardening models (Chapter 2).

---

1 R is the load ratio. With a stress (or strain) controlled amplitude it is defined by $R = \sigma_{min}/\sigma_{max}$ (or $R = \varepsilon_{min}/\varepsilon_{max}$ for strain) where σ_{min} and σ_{max} (respectively ε_{min} and ε_{max}) are the minimum and maximum values of a cycle.

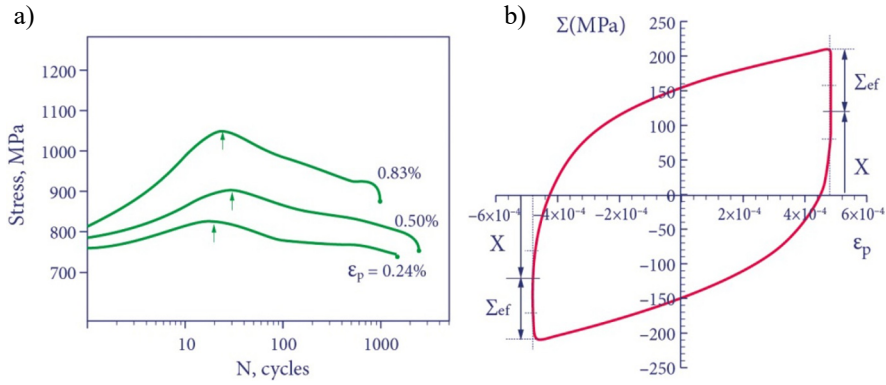

Figure 4.1. *a) Cyclic softening of a structural hardening nickel-based alloy (by [STO 78]); b) low-cycle fatigue hysteresis loop and the hardening kinematic (X) and isotropic (Σ_{ef}) components (from [HAD 04])*

The understanding of the various cyclic hardening stages requires that the microstructure be studied using transmission electron microscopy (TEM) to observe the evolution of the dislocation structures during accommodation. In the past, these studies have been conducted on FCC single crystals for which the hardening curves typically have three regimes according to the plastic deformation amplitude levels (Figure 4.2(a)). The TEM analyses show the presence of different dislocation structures according to the different regimes: vein structures for small strain levels; the coexistence in the plateau region of veins and structures which localize the plastic deformation (persistent slip bands (PSB)), with an increasing volume fraction of PSB when the strain level increases; and cells when slip multiplicity increases (higher strain levels).

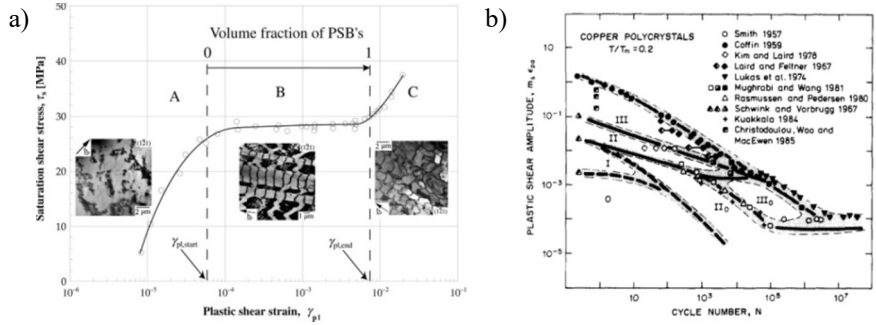

Figure 4.2. *a) Cyclic hardening curve (monocrystalline copper). Micrographs of the typical dislocation structures shown for the three regimes (by [PER 14]); b) fatigue mechanism map (polycrystalline copper) (by [PED 90])*

These studies have provided a framework which has been widely used to understand, at the microscopic scale, the hardening of polycrystalline alloys, made more complex by the effects of grain sizes, internal stresses, elastic anisotropy and texture [PER 14]. The great diversity of dislocation structures encountered can be more easily understood by representing the fatigue data on a map (N: number of cycles, plastic shear strain amplitude) [PED 90] (Figure 4.2(b)), where each region of the space can be associated with one or more characteristic dislocation structures (see Chapter 17 for more details).

4.2.2.2. *Damage mechanisms*

Low-cycle fatigue damage mechanisms rely on the same elements as cyclic hardening in a continuum of mechanisms [SAN 13]. During the cycles, the alternating movement of the dislocations leads to the formation of configurations that minimize their stored energy (e.g. PSBs). It can also lead to the creation of dislocations of opposite signs which, upon recombination, induce the creation of vacancies. The localized deformation bands (PSB, SB^2) are therefore the source of important incompatibilities (hard phase in a soft matrix) and of the flow of vacancies. The dislocations' movement is not perfectly reversible; we refer to the irreversibility of the plastic deformation. Changes in dislocation structures in the material's bulk are accompanied by the modification of the test specimen's surface relief (Figure 4.3), with the production of extrusions and often intrusions (part of material emerging above or below the average surface). These surface reliefs are known to be the preferred sites for crack initiation, and where the effect of the environment is important (see Chapter 17).'

4.2.2.3. *Low-cycle fatigue life law*

Although the understanding of initiation mechanisms is an important issue, the initiation phase in low-cycle fatigue is only a minor proportion of the total life [SUR 98]. From a more macroscopic point of view, it seems necessary to have laws to evaluate a material's *fatigue life*. Based on this observation, Manson and Coffin found, through the exploitation of much test data, that it is possible to relate the total fatigue life, N_f, to the plastic deformation amplitude, $\Delta_{\varepsilon p}/2$ (*Manson–Coffin law*):

$$\frac{\Delta\varepsilon_p}{2} = \varepsilon'_f N_f^c \qquad [4.1]$$

ε'_f and c are respectively the coefficient and the exponent of fatigue ductility, where c lies between –0.8 and –0.5 depending on the stress conditions and the material. When this empiric Manson–Coffin law is restricted to the initiation life,

2 Slip band.

then it can be related to active microstructural mechanisms and parameters during this damaging initiation phase [ALU 04, HO 17].

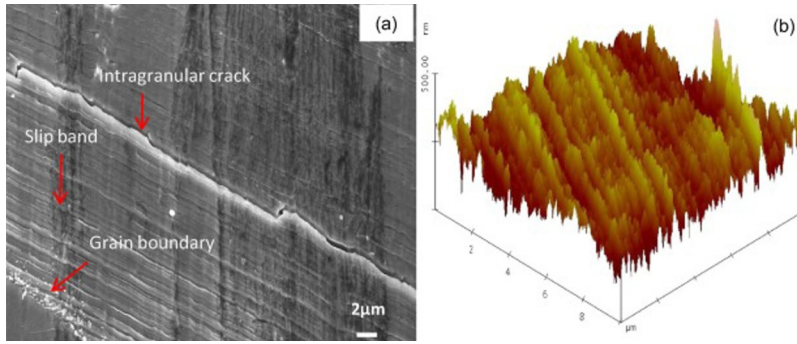

Figure 4.3. *Microstructure of the damaged surface of a nickel-based superalloy in low-cycle fatigue. a) SEM micrograph and b) surface topography obtained with atomic force microscopy [HO 17]. For a color version of this figure, see www.iste.co.uk/blanc/coupling.zip*

4.3. High-cycle and very high-cycle fatigue

4.3.1. *High-cycle fatigue tests*

The most common fatigue tests aim at determining the Wöhler curves (Figure 4.4) under constant amplitude sinusoidal loads (tension, compression, bending, torsion, etc. or a combination thereof) for different values of the load ratio R. These tests can be carried out on machines with operating frequencies which vary according to the technology used: servo-hydraulic (0 to ~ 50 Hz), electromagnetic vibrophore type (40 to ~ 250 Hz), electrodynamic (40 to ~ 300 Hz) and electrical (0 to ~ 300 Hz). Finally, given that tests in the gigacycle regime are very long on hydraulic or mechanical machines, piezoelectric testing machines operating in the ultrasound domain (typically 20 or 30 kHz) have been developed[3].

In order to obtain a Wöhler curve, the initiation of the fatigue crack(s) needs to be detected as soon as possible to avoid taking into account the propagation phase in the fatigue life. This detection is often done by monitoring the specimen's stiffness variation which, in general, makes it possible to detect cracks of a size greater than or equal to 1 mm. Another effective technique is the monitoring of the electrical potential during the test; however, this requires welding electrodes onto each test specimen, and so takes longer to implement.

3 Ultrasonic testing cannot always be used because of the high self-heating and the frequency effect which is sometimes induced [GUE 14].

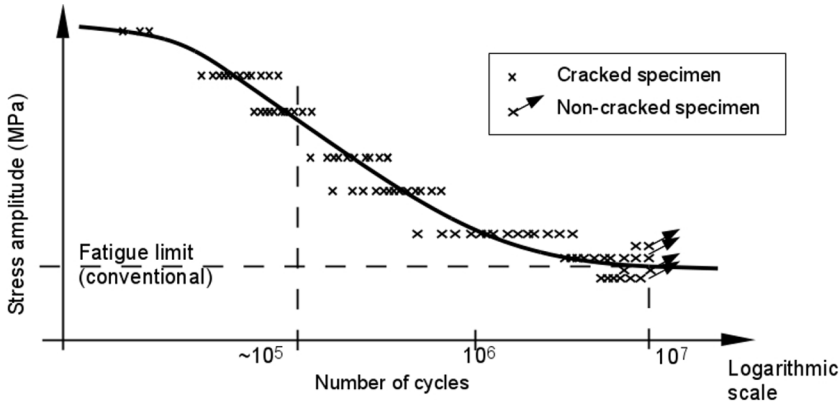

Figure 4.4. *Illustration of a typical Wöhler curve*

4.3.2. *Crack initiation, influence parameters*

In a high-cycle fatigue regime, without significant internal defects (refer to Kitagawa [KIT 76] for the consideration of defects), fatigue crack initiation occurs on the material's surface [SUR 98, BAT 10]. The surface and subsurface play a major role for several reasons. The roughness significantly influences the fatigue behavior given the high stress concentration that the grooves on the surface represent. The manufacturing processes generally harden the surface layers, or even create micro-damages, and they sometimes lead to phase transformations while most of the time they entail residual stresses. Residual stresses play a very important role in fatigue strength: tension stress reduces the resistance, while it increases it if it is compressive stress. On the other hand, since the surface is in contact with the external environment, the physicochemical interactions between the material and its environment play an important role in the crack initiation and propagation mechanisms [KRU 07] (see Chapters 16 and 17).

4.3.3. *Multiaxial fatigue*

Most components are subject to complex multiaxial loadings. Knowledge of the fatigue strength under simple loads is therefore not sufficient to predict their resistance in real conditions. The transfer of laboratory data to components under service loading is a separate field outside the scope of this chapter. Many factors must be taken into account: notches, metallurgical defects, surface condition, residual stresses, hardening of the surface layers, temperature, gradients of

mechanical properties, environment, etc. [BAT 10]. However, the initiation of a fatigue crack mainly depends on the state of local stresses (and strains). The stress tensor's multiaxial nature (more than one non-zero principal stress during a loading cycle) must be taken into account; this is known as multiaxial fatigue. Characterization tests are carried out on test apparata that make it possible to apply combined loads: tension-torsion, bending-torsion, tension-internal pressure on a thin wall tube, biaxial tension on a cruciform specimen, etc. [LIE 82].

4.3.3.1. *High-cycle multiaxial fatigue strength criteria*

In order to predict the resistance to fatigue crack initiation under multiaxial stress states in high-cycle fatigue regime, the endurance limit concept [HEN 05] defined for uniaxial stress is extended to these cases by establishing a fatigue criterion. By analogy with the yield strength criteria (von Mises, Tresca) it is a matter of choosing a relevant scalar parameter (equivalent stress or strain, volumetric energy density) calculated on a single loading cycle which is representative of the fatigue crack initiation phenomenon. Initiation occurs if this parameter exceeds a characteristic threshold for the material (Figure 4.5).

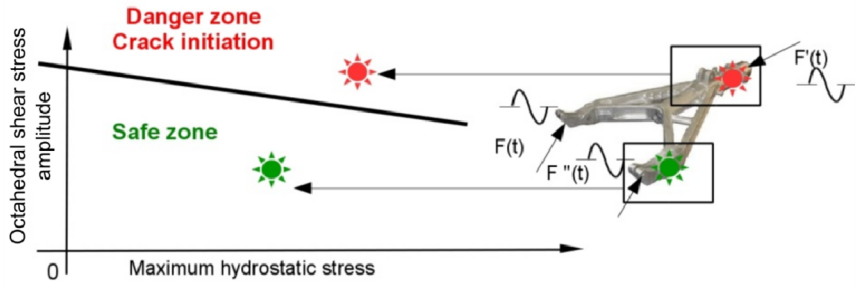

Figure 4.5. *Diagram illustrating the application of a high-cycle multiaxial fatigue strength criterion on a component. This one shows Crossland's. For a color version of this figure, see www.iste.co.uk/blanc/coupling.zip*

A multiaxial fatigue criterion can be formulated according to [4.2], linking an intrinsic constant to the material and a mathematical function, f, dependent on the stress tensor $\underline{\underline{\Sigma}}(\boldsymbol{M},\boldsymbol{t})$, and/or the strain tensor at the point M considered, $\underline{\underline{\epsilon}}(\boldsymbol{M},\boldsymbol{t})$:

$$\boldsymbol{f}\left(\underline{\underline{\boldsymbol{\Sigma}}}(\boldsymbol{M},\boldsymbol{t}),\underline{\underline{\boldsymbol{\epsilon}}}(\boldsymbol{M},\boldsymbol{t})\right) \leq \boldsymbol{Cte} \qquad [4.2]$$

It has been shown [CRO 59] that hydrostatic pressure (negative hydrostatic stress) prevents or delays the initiation and development of microcracks. In general,

the multiaxial fatigue criteria involve the hydrostatic part of the stress tensor in addition to a quantity related to the deviatoric part (see plasticity criterion). The usual criteria have two variables and can be illustrated on a plane (Figure 4.5). There are over 50 criteria in the literature [PAP 97, MAC 99], and the two most commonly used are shown hereafter.

To express the significant role of the deviatoric stress range (responsible for cyclic shear) on the initiation of a fatigue crack, Crossland [CRO 59] proposed to use the octahedral shear stress range $\boldsymbol{\tau_{oct,\Delta J2}}$ as a variable, linearly combined at the maximum hydrostatic stress over a cycle, $\boldsymbol{\sigma_{H,max}}$. At every point M, this criterion is:

$$\tau_{oct,\Delta J2}(M) + \alpha\, \sigma_{H,\max}(M) \leq \beta \qquad [4.3]$$

where $\tau_{oct,\Delta J2} = \frac{1}{2}\sqrt{\underset{t1}{max}\left[\underset{t2}{max}\left\{J_2\left(\underline{\underline{\Sigma}}(M,t_1)\right) - J_2\left(\underline{\underline{\Sigma}}(M,t_2)\right)\right\}\right]}$, and $J_2(M,t)$ is the second invariant of the deviatoric part, $\underline{\underline{\boldsymbol{S}}}$, of the stress tensor, $\underline{\underline{\boldsymbol{\Sigma}}}$, and $\sigma_{H,max} = \underset{t}{max}\left[\frac{1}{3} trace\left(\underline{\underline{\Sigma}}(M,t)\right)\right]$. α and β are material parameters identified from two experimental fatigue limits obtained from test specimens without stress concentration, without residual stresses and with a polished surface.

Dang Van [DAN 99] was the first to propose a two-scale micromechanical approach. This approach accounts for the fact that in the long-life regime, the material remains macroscopically elastic. The cyclic plasticity appears on the mesoscopic scale (the scale of grains) to give rise to persistent slip bands on the surface of the material, which are the precursors of microcracks. This approach has paved the way for several other criteria [PAP 94, PAP 97, MOR 98] and for polycrystalline modeling of the high-cycle fatigue strength of metals. Dang Van assumes that the representative volume element (RVE) on which the constraints are calculated during a structural computation consists of a large number of equiprobable random orientation grains. These grains are supposed not to crack under cyclic loading if, and only if, there is an elastic shakedown.

We can therefore show [DAN 99] that after enough cycles, the mesoscopic stress field is given by: $\underline{\underline{\boldsymbol{\sigma}}}(\boldsymbol{t}) = \underline{\underline{\underline{\underline{\boldsymbol{A}}}}} : \underline{\underline{\boldsymbol{\Sigma}}}(\boldsymbol{t}) + \underline{\underline{\boldsymbol{\rho}}}^*$ where $\underline{\underline{\underline{\underline{\boldsymbol{A}}}}}$ is the localization tensor and $\underline{\underline{\boldsymbol{\rho}}}^*$ a time-independent residual stress field. Fatigue crack initiation occurs in unfavorably oriented grains during a stress cycle if the mesoscopic plasticity criterion $\boldsymbol{f}\left(\underline{\underline{\boldsymbol{\sigma}}}(\boldsymbol{t})\right) < 0$, is violated. The plasticized grain where the fatigue crack will initiate is then embedded in a set of elastic grains (or elastic matrix). In order to explain the experimental results, in particular the role of hydrostatic stress in high-cycle fatigue,

Dang Van assumes that the mesoscopic plasticity criterion is a linear combination of the norm of the mesoscopic shear stress vector in the elastic-shakedown state, $\boldsymbol{\tau}(\vec{n}, t)$, on a crystallographic plane of unit normal, $\vec{n}$, and the mesoscopic hydrostatic stress, $\sigma_H(t)$:

$$\max_{\vec{n}}\left[\max_{t}\left(\|\boldsymbol{\tau}(\vec{n}, t)\| + a\sigma_H(t)\right)\right] \leq b \qquad [4.4]$$

It has been shown by [DAN 99] and [HEN 05] that the hydrostatic stress is identical on both the macroscopic and mesoscopic scales, $\boldsymbol{\sigma_H} = \boldsymbol{\Sigma_H}$. In general, the application of criterion [4.4] requires the search for a double maximum (with respect to $\vec{n}$ and t). For each plane with normal $\vec{n}$, the search for the norm of the adapted mesoscopic shear stress vector is done through the construction of the smallest circle circumscribed to the path described by the end of the macroscopic shear vector, $\vec{C}(t) = \underline{\Sigma}(t) \cdot \vec{n} - \vec{n} \cdot \underline{\Sigma}(t) \cdot \vec{n}$, on the considered plane. a and b are two parameters of the material identified according to two median fatigue limits such as in Crossland's case.

4.3.3.2. *Probabilistic approaches in high-cycle fatigue*

Since the initiation of fatigue cracks is a very scattered phenomenon (Figure 4.4), it is better to speak of a P-S-N curve (which stands for "Probability – Stress – Number of cycles") and fatigue strength for a survival probability before a given number of cycles. Several authors have proposed probabilistic models[4]. The reader who wishes to go into greater depth in this topic can check the following references: [CHA 99, DEL 06, PES 11].

4.3.4. *A few words on gigacycle fatigue*

The concept of the Wöhler curve proposed at the end of the 19th Century has, for a long time, been limited to 10^7 cycles given the length of the test durations. This curve's asymptotic trend has led many authors to assume the existence of a limit stress amplitude below which the material could withstand an "infinite" number of cycles. Towards the end of the 20th Century, it was proved that an "infinite" life does not exist [BAT 99, NIS 99, WAL 00] and that crack initiation mechanisms change when the loading level decreases from 10^7 to 10^9 cycles and more. This means moving from surface crack initiation to internal crack initiation, usually on non-metallic inclusions [MUR 00], but not always [NIK 16]. The concept of

4 More precisely, semi-probabilistic. In fact, in a probabilistic model the resistance properties and the loading need to be probabilized.

fatigue criterion is therefore limited to a long fatigue life of between 10^6 and 10^7 cycles, but cannot be directly extended beyond that given that the initiation mechanisms are different. These mechanisms are still poorly understood and are the subject of research.

4.4. Fatigue crack propagation

4.4.1. *Characterization of fatigue crack growth resistance*

In order to characterize the fatigue crack growth resistance of a given material, crack propagation tests are usually carried out on pre-cracked standard fracture mechanics test specimens (MT, CT, SEN, etc.), which are generally subjected to mode I loading, with load control and at a constant frequency [AST 08]. The pre-cracking phase is necessary to initiate a crack from a mechanical notch in order to then allow the crack to get out from the area affected by the plasticity generated around this notch. The main techniques used to monitor the crack length during the test are: 1) an optical measurement on a polished face of the test piece; 2) a measurement of the specimen compliance using a crack-opening displacement sensor mounted at the crack mouth or a back-face strain gauge [SAX 78]; 3) an electric potential drop technique which requires a prior calibration of the relationship between the potential and the crack length [JOH 65].

The raw test results give the evolution of the crack length, a, as a function of the number of cycles N, from which the crack propagation rate denoted as da/dN can be derived.

4.4.2. *Using fracture mechanics concepts – the concept of ΔK*

The a-f(N) data thus generated strongly depend on the test conditions such as the size and geometry of the test specimen, the amplitude of the stress applied, the initial crack length, etc. This barrier was overcome by Paris *et al*. [PAR 63], who showed that the linear elastic fracture mechanics parameters make it possible to rationalize the propagation data established for different experimental conditions. They introduced the notion of the stress intensity factor range, defined as follows:

$$\Delta K = K_{max} - K_{min} = K_{max} \times (1 - R) \qquad [4.5]$$

where K_{max} and K_{min} are respectively the maximum and minimum values of the stress intensity factor K during the cycle and R is the load ratio. The use of the stress intensity factor, K, is based on the same assumptions as in the case of linear elastic

fracture mechanics, namely that the crack tip plasticity must remain confined in a small volume compared to the other problem dimensions. When analyzing the results of a crack propagation test by calculating the value of ΔK (function of the variation of the stress range far from the crack, $\Delta\sigma$, and the crack length a) corresponding to the measured crack propagation rates da/dN, the data collected for the different test conditions are grouped around the same average curve. This analogy principle also makes it possible to transfer the data obtained from laboratory test specimens to structural calculations, which is the basis of the damage tolerance approaches.

The fatigue crack growth resistance of a given alloy for specific stress conditions (load ratio, temperature, environment, sampling direction, etc.) is characterized by a curve plotted in a bi-logarithmic diagram. The general appearance shown in Figure 4.6 consists of three characteristic regions. Region I is characterized by a fast decrease of the crack growth rate when ΔK approaches a characteristic value called the fatigue crack propagation threshold, $\Delta K_{threshold}$. Below this value, the damage generated at the crack tip by the cyclic loading is so small that it is almost impossible to experimentally detect any crack advance. This region is also characterized by a strong effect of the microstructure, the load ratio and the environment. In region II, or the Paris domain, the curve generally presents a linear section over a fairly wide range. This power law dependence of the fatigue crack propagation rate with respect to the amplitude of the stress intensity factor ΔK (Paris equation), is given by:

$$\boldsymbol{da/dN = C \times \Delta K^m} \qquad [4.6]$$

It is usually in region II where fatigue striations are observed [BOW 72, LAI 67, NEU 69, PEL 70], consisting of periodic markings with a spacing correlated with the macroscopic growth rate da/dN, reflecting a cycle-by-cycle progression of the crack. Finally, region III corresponds to an acceleration of the propagation just before the sudden rupture when K_{max} approaches a critical value characteristic of the fracture toughness of the material, K_c.

However, the behavior characterized by this curve (Figure 4.6) represents a global response resulting from different phenomena affecting it and which arise from factors with different physical origins among which we can distinguish factors intrinsic to the material (Young's modulus, elastic limit, cyclic behavior in relation to microstructural parameters, etc.) and *extrinsic* factors such as: load ratio (R), loading history and frequency, environment, temperature, thickness of the component, residual stress fields, etc.

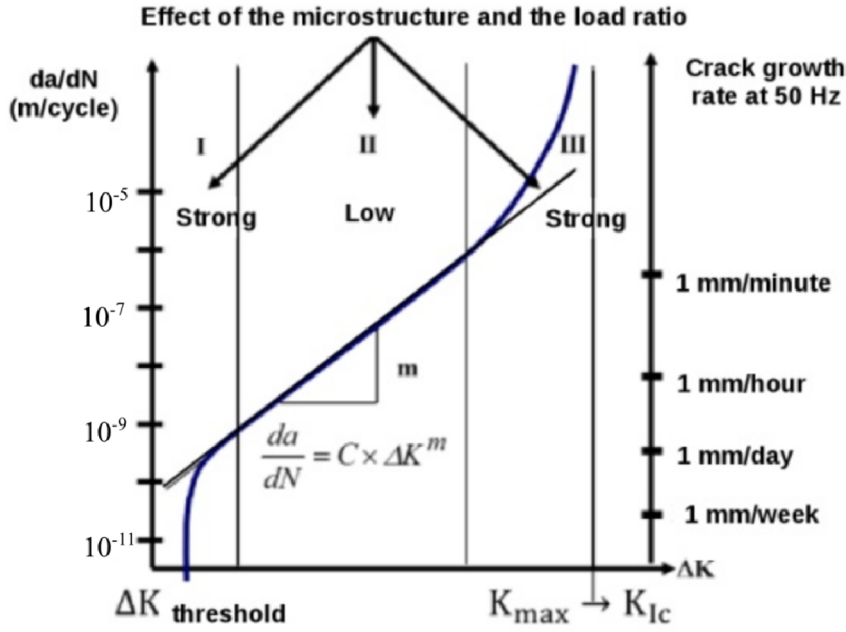

Figure 4.6. *da/dN versus ΔK plot showing the different propagation regimes*

4.4.3. *Monotonic and cyclic plastic zones*

The progression of a fatigue crack results from a damaging process at the crack tip, which is in turn related to the cyclic plastic deformation amplitude applied on the material in this region. This phenomenon is shown in Figure 4.7 with the assumption of a perfectly plastic elastic material for which the elastic limit in compression is equal to the opposite of the tension limit. Within the monotonic plastic region, a region of cyclic plastic deformations known as a cyclic plastic zone develops, as opposed to the monotonic plastic zone created during monotonic loading. The radius of this area is given by the equation:

$$\boldsymbol{r_{ZPc} = \alpha \times \left(\Delta K / 2\sigma_y\right)^2} \qquad [4.7]$$

In reality, the yield strength is not constant within the plastic zone and varies according to the strain hardening, which at least in part explains the disparities between experimental observations (micro-hardness, X-ray diffraction, TEM, etc.) and theoretical models.

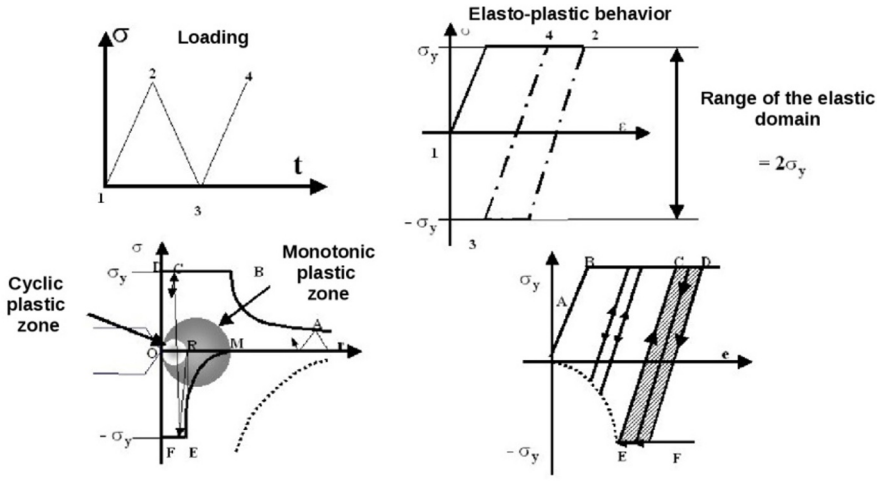

Figure 4.7. *Cyclic plastic deformations at crack tip*

4.4.4. *Effect of the R ratio, crack closure*

The effect of the R load ratio results in a shift of the da/dN-ΔK curves towards lower ΔK values for a given crack propagation rate as R increases. The $\Delta K_{threshold}$ value in particular strongly depends on the load ratio. The most widely accepted (though still controversial) explanation for this effect is based on the crack closure mechanism introduced by Elber [ELB 71], who experimentally demonstrated that a fatigue crack, even when subjected to cyclic tensile loading, could remain closed over a section of its length for a fraction of the fatigue cycle around the minimum load. Only the upper part of the cycle actually contributes to the propagation. Elber introduced the effective stress intensity factor range:

$$\Delta Keff = Kmax - Kop \qquad [4.8]$$

where K_{op} represents the stress intensity factor at the crack opening. Subsequent works have shown that the relationship between ΔK_{eff} and R is complex, especially close to the threshold where plasticity is no longer the single source of closure but where the environment and the microstructure influence the intensity of closure effects [SUR 83]. At first these effects were mainly associated with the planar stress states because it is more difficult to determine the closure effects in planar deformations, and because the theoretical models were limited to this state of constraints [BUD 78]. Experimental measurements, supported by numerical simulations, have confirmed that crack closure effects, although less intense, also affect propagation in planar deformations [FLE 88, POM 02, REI 98]. These effects

are extremely confined to the vicinity of the crack tip, making their experimental determination a delicate process. For a 3D crack, closure effects change from the surface (plane stress state) to the core where the behavior is dictated by the state of plane strains.

4.4.5. *Fatigue crack propagation laws*

A fatigue crack propagation law is a function relating da/dN to ΔK by eventually empirically taking into account the influence of different parameters. Thus, the C and m parameters of the Paris equation certainly depend on the material, but also on the test conditions (R ratio, environment, etc.). The extrapolation of such equations to different propagation conditions (small cracks, complex loading, slow frequency, etc.) must therefore be based on an understanding of physical mechanisms and requires experimental validation. A commonly used equation is the NASGRO equation [FOR 92, NAS 02] that describes the entire propagation region, from the crack propagation threshold to the final fracture while including the effect of the R ratio:

$$\frac{da}{dN} = C \times \left[\left(\frac{1-f}{1-R}\right)\Delta K\right]^n \left[\left(1 - \frac{\Delta K_{threshold}}{\Delta K}\right)^p \Big/ \left(1 - \frac{K_{max}}{K_{crit}}\right)^q\right] \quad [4.9]$$

Many theoretical approaches have been developed to provide a theoretical basis for these empirical formulations [CHA 93, ELL 97, ROV 91]. However, since these approaches do not generally explicitly take into account the environmental effect, they only apply, *a priori*, to the prediction of intrinsic propagation resistance, that is, without and/or corrected for closure effects and in an inert environment.

4.4.6. *Intrinsic resistance to fatigue cracking*

Three propagation modes have been identified in intrinsic fatigue crack growth [PET 00]. 1) Stage I is observed on single crystals and representative of the first stages of propagation of a surface microcrack [PET 92]. 2) Stage II, where the crack propagates perpendicular to the principal stress axis, is the most commonly observed, especially in the Paris region (Figure 4.8(a)). 3) The pseudo-stage I, with a marked crystallographic character, corresponds to a stage I propagation within a grain; near the grain boundary, the crack is stationary before propagating in the adjacent grain according to a plane differently oriented. The result of this is a zigzag crack path that, from a macroscopic point of view, is similar to that of stage II (Figure 4.8(b)). The microstructural barrier effect involved in pseudo-stage I results in a greatly reduced propagation compared to stage II. Intrinsic stage II is furthermore correctly described using crack tip cumulative damage models [PET 91].

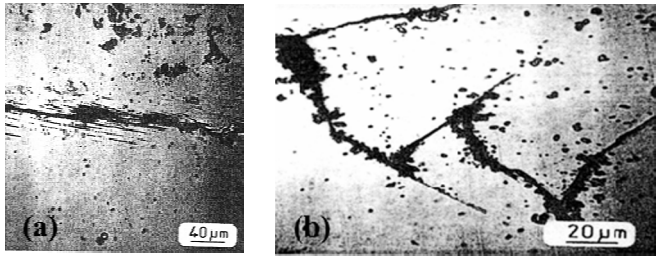

Figure 4.8. *Propagation in a vacuum-stressed 2024T351 aluminum alloy, a) in stage II, b) in pseudo-stage I (by [PET 00])*

4.4.7. *Fatigue crack propagation threshold – environment/closure/ microstructure interactions*

Given that the effect of the environment on crack growth rates by modifying the deformation and damage mechanisms is addressed elsewhere, here we are only interested in the interactions between the environment and other effects such as closure. Near threshold, the influence of the load ratio is increasingly important in connection with the greater contribution of the closure effects. In addition to the plastic-induced closure that prevails in the high ΔK region, other closure sources are effective (Figure 4.9), such as closure induced by the presence of an oxide film with a thickness of the same order of magnitude as the cyclic displacement of the crack lips, ΔCTOD, which develops on broken surfaces [BIG 90, PET 03, SUR 84, SUR 81]. Closure induced by the oxide induces a positive effect of the environment from the point of view of crack growth resistance. Another source of closure is the closure induced by the roughness of the surfaces [SUR 82, SUR 83].

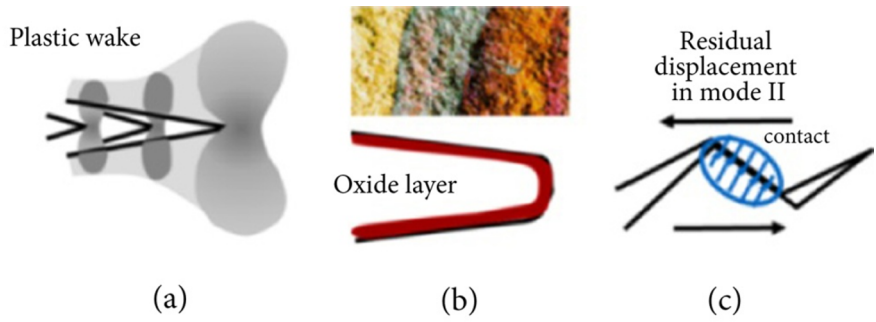

Figure 4.9. *Different crack closure mechanisms a) plasticity-induced closure; b) oxide-induced closure; c) roughness-induced closure. For a color version of this figure, see www.iste.co.uk/blanc/coupling.zip*

In practice, predicting the intensity of closure effects near the threshold as a function of the loading conditions is made difficult by the complexity of the processes involved [CHO 16]. Metallurgical factors, such as grain size, the nature and distribution of the precipitation, or the resulting elastoplastic stress-strain behavior, affect the propagation near the threshold. Thus, for a given value of R, the $\Delta K_{threshold}$ value increases as the grain size increases (Figure 4.10), which reflects the positive effect of grain coarsening related to the increase in closure effects since the value of $\Delta K_{eff,\ threshold}$ is independent of grain size [PIP 91]. This effect of the grain size on the intensity of the closure effects occurs through the roughness of the surfaces created, as well as by a yield strength effect.

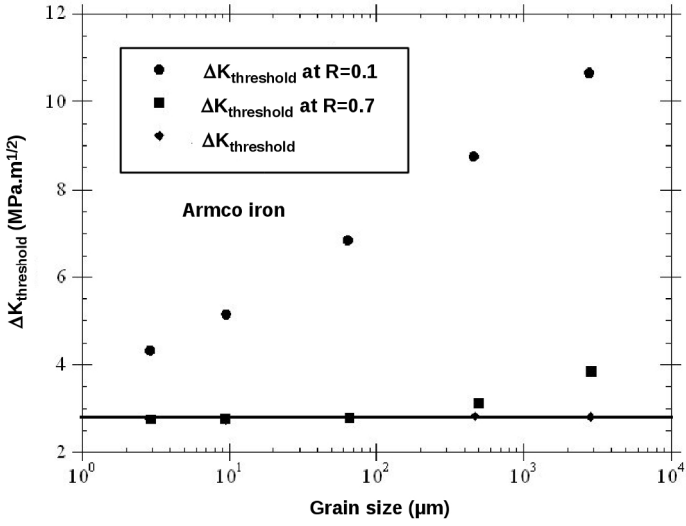

Figure 4.10. *Effect of the grain size on the $\Delta K_{threshold}$ value in pure iron (by [PIP 91])*

4.4.8. *Propagation of small cracks*

While propagation equations used in crack propagation computations are commonly based on fatigue crack growth rates measured on millimeter-sized cracks, in practice it may be necessary to consider much smaller cracks, for example in life-extension procedures. However, the fatigue crack propagation rates of small cracks can be much higher than those considered for long cracks with stress applied under the same conditions [PEA 75]. Thus, the use of long crack data can lead to significant overestimates of crack-propagation life. As an example of short crack behavior (Figure 4.11(a)), a minimum speed is observed when the crack size is comparable to the grain size, suggesting a microstructural barrier role played by the grain boundaries [LAN 82].

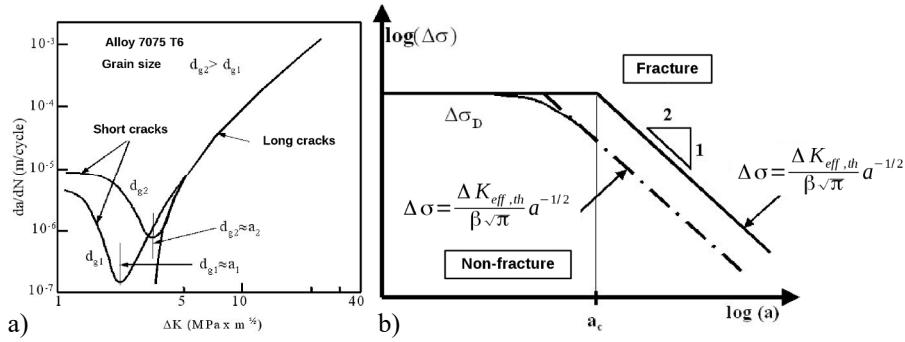

Figure 4.11. *a) Effect of the grain size on the behavior of short cracks in the 7075 T6 alloy [LAN 82]; b) the Kitagawa–Takahashi diagram [KIT 76]*

The problem of short cracks can also be seen as a problem of non-compliance with small-scale yielding conditions when the defect size is small compared to the plastic zone size. Moreover, other terms such as the T stress which also influence the development of the plastic wake, and therefore the development of the closure effects, should be included in the calculation of the stress/strain fields in the vicinity of the short crack tip [FLE 88]. Short cracks are subjected to lower wake effects that become active only as the crack grows [VOR 13a, VOR 13b]. Then, the behavior of the small crack gradually resembles that established for a long crack. The difference in propagation speed between short and long cracks also generally considerably diminishes as soon as these speeds are expressed as a function of ΔK_{eff}.

In addition, Kitagawa and Takahashi [KIT 76] showed that there is a critical defect size below which the fatigue limit is independent of the defect size. Above this size, the propagation condition of a defect is controlled by the value of $\Delta K_{threshold}$ or $\Delta K_{threshold,\ eff}$. The Kitagawa–Takahashi diagram (Figure 4.11(b)) therefore separates a non-failure domain from a failure domain by joining two straight lines where their intersection corresponds to the critical defect size, a_c.

4.5. Mixed-mode fatigue crack growth

The "classical" bifurcation criteria (maximum tangential stress, maximum energy release rate, local symmetry, etc.) predict that a crack submitted to shearing or opening + shearing, immediately changes its propagation plane to recover a pure mode I. This is true for most cases. However, there are significant exceptions where a macroscopic propagation in modes II or III is observed. These are essentially torsion or pure shear cyclic loading, or complex stresses with a strong hydrostatic compression that tend to inhibit the opening of cracks, such as in rolling contact fatigue.

4.5.1. *Fatigue cracking in mode III*

Hourlier and Pineau [HOU 82], Brown *et al*. [BRO 85] as well as Tschegg and Stanzl [TSC 88] conducted alternating torsion tests, on circumferential notched cylindrical steel specimens, leading to mode III along the (circular) front of the crack. Although the amplitude ΔK_{III} was kept constant, the propagation velocity decreased (Figure 4.12(a)). If a static axial tension (which induces mode I) was added, the deceleration was less pronounced the larger K_I was. If, on the other hand, static compression was applied, the deceleration was emphasized (Figure 4.12(b)).

The origin of the deceleration is therefore the progressive increase of the energy dissipated by the friction of crack lips as its depth increases (and with it, the contact surface), to the detriment of the energy available to create new crack surfaces. The apparent value of ΔK_{III}, calculated for a smooth and frictionless crack ($\Delta K_{III}^{nominal}$), doesn't account for the real singularity at the crack tip which is reduced by friction to a decreasing $\Delta K_{III}^{effective}$ value. It can be seen in Figure 4.12(b) that for the same ΔK_{III}, the propagation rates extrapolated to a zero crack depth are similar, whatever the normal loading is. It is therefore logical to consider this to be an intrinsic rate (i.e. not affected by friction) and to plot the two values (extrapolated rate – ΔK_{III}) on a da/dN-$\Delta K_{III}^{effective}$ diagram (Figure 4.12(c), on which the kinetic curve for mode I has also been plotted).

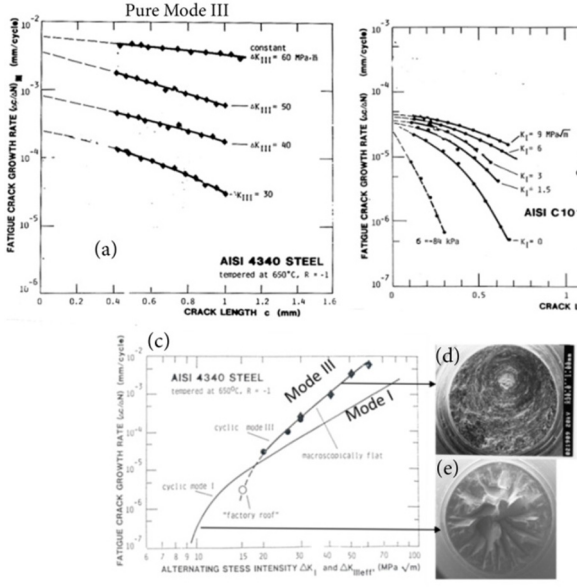

Figure 4.12. *Evolution of crack depths during testing at constant $\Delta K_{III}^{nominal}$ a) without or b) with axial stress. c) Intrinsic cracking kinetics in modes I and III and corresponding fracture surfaces (d, e) (by [TSC 83])*

The kinetic cracking curves in modes I and III intersect at a point above which mode III cracking is the fastest and below which mode I cracking is the fastest. Moreover, this intersection point corresponds to a change of fracture facies: flat and smooth (with tangential traces of friction) above and a "factory roof morphology" below (Figures 4.12(d, e)). The latter facies correspond to a local twisting of the crack by ± 45° which makes it experience a mode I loading. The studies by the teams mentioned above agree on the idea that a fatigue crack propagates according to the mode (opening or shearing) for which it has a maximum rate. Unlike conventional bifurcation criteria, it does not exclude the possibility of cracking in shear mode.

4.5.2. *Fatigue cracking in mode II*

The works of Smith *et al*. [SMI 88], Otsuka *et al*. [OTS 80] as well as Doquet and Bertolino [DOQ 08] have shown that in modes II and III, the contact and friction of the crack micro-asperities 1) induce the wearing of fracture facets, covered with oxidized metal debris (Figure 4.13(a)); 2) gradually reduce the effective value of the stress intensity factor; and 3) lead to a deceleration followed by a bifurcation in tests conducted at constant $\Delta K_{II}^{nominal}$. Once again, the da/dN-$\Delta K_{II}^{effective}$ curves corrected for friction effects (Figure 4.13(b)) cross over the mode I kinetic curves with, at high ΔK_{II}, a regime in which mode II propagation can be observed; on the other hand, below the point of intersection, the crack bifurcates to propagate in mode I, according to the criterion of maximum rate.

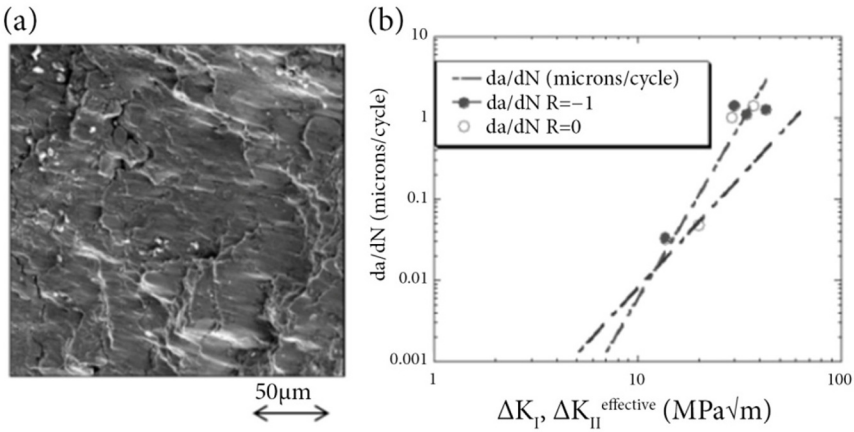

Figure 4.13. *a) Fracture surface in mode II of a ferrite-pearlite steel and b) cracking intrinsic kinetics in modes I and II [DOQ 04]. For a color version of this figure, see www.iste.co.uk/blanc/coupling.zip*

4.5.3. *Interaction between modes*

The decrease (respectively, the increase) of the friction effects induced by mode I loading (respectively, normal compression) superimposed on a shear load has already been mentioned in this chapter. Conversely, a static loading in mode II or III (superimposed to cyclic mode I) by laterally shifting the crack lip asperities causes their premature contact upon unloading, increasing asperities-induced closure effects and decelerating the propagation in mode I [STA 89]. Complex interactions between modes I, II and III are also seen in terms of crack tip plasticity: the presence of a mode II static loading in addition to a cyclic mode I loading reduces plasticity-induced closure effects [DOQ 10]. Non-proportional mixed mode cracking paths and speeds depend not only on the magnitude of the $\Delta K_I^{effective}$, $\Delta K_{II}^{effective}$ and $\Delta K_{III}^{effective}$, but also on the shape of the loading path in a $K_I(t)$, $K_{II}(t)$, $K_{III}(t)$ space [FRE 14, DOQ 09].

4.5.4. *Effect of the environment on the crack path*

Vogelesang *et al*. [VOG 80] and Esnault *et al*. [ESN 14] have shown that the environment can affect not only the crack propagation speed, but also its path. A crack in a thin sheet of metal with stress in cyclic mode I gradually twists via the development of shear lips (Figure 4.14(a)), therefore switching from mode I to a mode I+II+III. For a 7075 aluminum alloy, the ΔK_I value for which crack twisting is total is lower in a vacuum than in air, and larger in a saline solution (Figure 4.14(b)). The maximum rate criterion, provided that it relies on kinetic cracking data in modes I, II or III in a medium representing the service conditions, can account for the environmental effects on the preference for one or another propagation mode [DOQ 08].

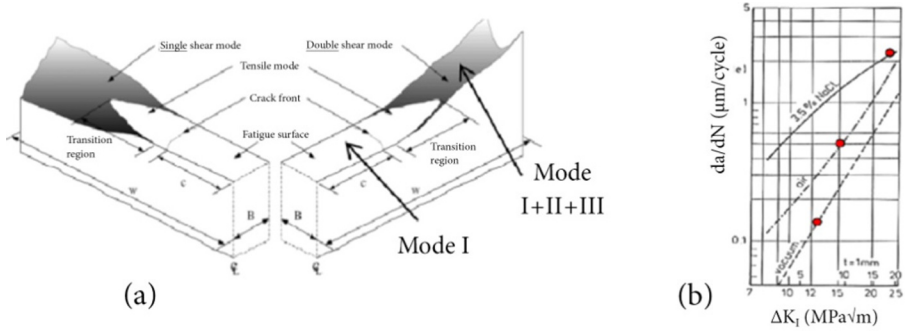

Figure 4.14. *a) Typical fatigue cracking paths in a thin metal sheet. b) Cracking kinetics of an Al 7075 alloy in three different environments. The three large dots represent full twisting [VOG 80]*

4.6. References

[ALU 04] ALUSH H., KATZ Y., MAROS M.B. *et al.*, "Some insights into the remote strain versus fatigue life relationship", *Journal of Materials Processing Technology*, vols 157–158, pp. 16–22, 2004.

[AST 08] ASTM, E647-05 standard test method for measurement of fatigue crack growth rates, 2008.

[BAT 99] BATHIAS C., "There is no infinite fatigue life in metallic materials", *Fatigue & Fracture of Engineering Materials & Structures*, vol. 22, pp. 559–565, 1999.

[BAT 10] BATHIAS C., PINEAU A., *Fatigue of Materials and Structures: Fundamentals*, ISTE Ltd, London and John Wiley & Sons, New York, 2010.

[BRO 85] BROWN M.W., HAY E., MILLER K.J., "Fatigue at notches subjected to reversed torsion and static axial loads", *Fatigue & Fracture of Engineering Materials & Structures*, vol. 8, p. 243, 1985.

[CHA 93] CHAN K.S., "Scaling laws for fatigue crack growth of large cracks in steels", *Metall. Trans*., vol. 24A, pp. 2473–2485, 1993.

[CHA 99] CHANTIER I, BOBET V, BILLARDON R. *et al.*, "A probabilistic approach to predict the very high-cycle fatigue behaviour of spheroidal graphite cast iron structures", *Fatigue & Fracture of Engineering Materials & Structures*, vol. 23, pp. 173–80, 1999.

[CHO 16] CHOWDHURY P., SEHITOGLU H., "Mechanisms of fatigue crack growth – a critical digest of theoretical developments", *Fatigue & Fracture of Engineering Materials & Structures*, vol. 39, pp. 652–674, 2016.

[CRO 59] CROSSLAND B., "Effect of a large hydrostatic pressure on the torsional fatigue strength of an alloy steel", *Int. Conf. Fatigue of Metals*, pp. 138–149, London, 1959.

[DAN 99] DANG VAN K., PAPADOPOULOS I.V., *High-Cycle Metal Fatigue – From Theory to Applications*, Springer-Verlag, 1999.

[DEL 06] DELAHAY T., PALIN-LUC T., "Estimation of the fatigue strength distribution in high-cycle multiaxial", *Int. J. Fatigue*, vol. 28, pp. 474–484, 2006.

[DOQ 08] DOQUET V., BERTOLINO G., "A material and environment-dependent criterion for the prediction of fatigue crack paths in metals", *Engineering Fracture Mechanics*, vol. 75, no. 11, pp. 3399–3412, 2008.

[DOQ 09] DOQUET V., ABBADI M., BUI Q.H. *et al*., "Influence of the loading path on fatigue crack growth under mixed-mode loading", *Int. J. Fracture*, vol. 159, pp. 219–232, 2009.

[DOQ 10] DOQUET V., BUI Q.H., CONSTANTINESCU A., "Plasticity and asperity-induced fatigue crack closure under mixed-mode loading", *Int. J. Fatigue*, vol. 32, no. 10, pp. 1612–1619, 2010.

[ELB 71] ELBER W., "The significance of crack closure", in ROSENFELD M.S. (ed.), *Damage Tolerance in Aircraft Structures*, ASTM STP, vol. 486, 1971.

[ELL 97] ELLYIN F., *Fatigue Damage, Crack Growth and Life Prediction*, Chapman & Hall, 1997.

[ESN 14] ESNAULT J.B., DOQUET V., MASSIN P., "A three-dimensional analysis of fatigue crack paths in thin metallic sheets", *Int. J. Fatigue*, vol. 62, pp. 119–132, 2014.

[FLE 88] FLECK N.A., NEWMAN J.C.J., "Analysis of crack closure under plane strain conditions", in NEWMAN J.C.J., ELBER W. (eds), *Mechanics of Fatigue Crack Closure*, ASTM STP, Philadelphia, vol. 982, 1988.

[FOR 92] FORMAN R.G., METTU S.R., "Behavior of surface and corner cracks subjected to tensile and bending loads in Ti-6al-4v alloy", in ERNST H.A., SAXENA A., MCDOWELL D.L. (eds), *Fracture Mechanics: Twenty-second Symposium*, ASTM STP, Philadelphia, vol. 1131, 1992.

[FRE 14] FREMY F., POMMIER S., PONCELET M. *et al.*, "Load path effect on fatigue crack propagation in I + II+ III mixed mode conditions", *Int. J. Fatigue*, vol. 62, pp. 104–118, 2014.

[GUE 14] GUENNEC B., UENO A., SAKAI T. *et al.*, "Effect of the loading frequency on fatigue properties of JIS S15C low carbon steel and some discussions based on micro-plasticity behavior", *Int. J. Fatigue*, vol. 66, pp. 29–38, 2014.

[HAD 04] HADDOU H., RISBET M., MARICHAL G. *et al.*, "The effects of grain size on the cyclic deformation behaviour of polycrystalline nickel", *Materials Science and Engineering: A*, vol. 379, pp. 102–111, 2004.

[HEN 05] HENAFF G., MOREL F., *Fatigue des structures*, Eyrolles, 2005.

[HER 11] HERBIG M., KING A, REISCHIG P. *et al.*, "3-D growth of a short fatigue crack within a polycrystalline microstructure studied using combined diffraction and phase-contrast X-ray tomography", *Acta Materialia*, vol. 59, no. 2, pp. 590–601, 2011.

[HO 17] HO H.S., RISBET M., FEAUGAS X., "A cyclic slip irreversibility based model for fatigue crack initiation of nickel base alloys", *Int. J. Fatigue*, vol. 102, pp. 1–8, 2017.

[HOU 82] HOURLIER F., PINEAU A., "Propagation of fatigue cracks under polymodal fatigue", *Fatigue & Fracture of Engineering Materials & Structures*, vol. 5, no. 4, pp. 287–302, 1982.

[ISO 17] ISO 12106:2017, Metallic materials – Fatigue testing – Axial-strain-controlled method, March 2017.

[JOH 65] JOHNSON H.H., "Calibrating electric potential method for studying slow crack growth", *Materials Research and Standards*, vol. 5, p. 442, 1965.

[KIT 76] KITAGAWA H., TAKAHASHI S., "Applicability of fracture mechanics to very small cracks or the cracks in the early stage", *Second International Conference on Mechanical Behavior of Materials*, vol. 25, pp. 627–631, 1976.

[KON 88] DE KONING A.U., DOUGHERTY D.J., "Prediction of low and high crack growth rates under constant and variable amplitude loading", in PETIT J., DAVIDSON D.L., SURESH S. *et al*. (eds), *Fatigue Crack Growth Under Variable Amplitude Loading*, Elsevier Applied Science**,** London, 1988.

[KRU 07] KRUPP U., *Fatigue Crack Propagation in Metals and Alloys*, Wiley-VCH, 2007.

[LAI 67] LAIRD C., "The influence of metallurgical structure on the mechanisms of fatigue crack propagation", in GROSSKREUTZ J. (ed.), *Fatigue Crack Propagation*, ASTM STP, vol. 415, 1967.

[LAN 82] LANKFORD J., "The growth of small fatigue cracks in 7075-T6 aluminum", *Fatigue of Engineering Materials and Structures*, vol. 5, pp. 233–248, 1982.

[LIE 82] LIEURADE H.-P., *La pratique des essais de fatigue*, PYC Editions, 1982.

[MAC 99] MACHA E., SONSINO C.M., "Energy criteria of multiaxial fatigue failure", *Fatigue & Fracture of Engineering Materials & Structures*, vol. 22, no. 12, pp. 1053–1070, 1999.

[MOR 98] MOREL F., "A fatigue life prediction method based on a mesoscopic approach in constant amplitude multiaxial loading", *Fatigue & Fracture of Engineering Materials & Structures*, vol. 21, no. 2, pp. 41–56, 1998.

[MUR 00] MURAKAMI Y., NOMOTO T., UEDA T., "On the mechanism of fatigue failure in the superlong life regime (N >107 cycles). Part II: A fractographic investigation", *Fatigue & Fracture of Engineering Materials & Structures*, vol. 23, pp. 901–910, 2000.

[NAS 02] NASGRO, Nasgro fracture mechanics and fatigue crack growth analysis software, NASA, San Antonio, 2002.

[NEU 69] NEUMANN P., "Coarse slip model of fatigue", *Acta Metallurgica*, vol. 17, pp. 1219–1225, 1969.

[NIK 16] NIKITIN A., PALIN-LUC T., SHANYAVSKIY A, "Crack initiation in VHCF regime on forged titanium alloy under tensile and torsion loading modes", *Int. J. of Fatigue*, vol. 93, pp. 318–325, 2016.

[NIS 99] NISHIJIMA S., "Stepwise S-N curve and fish-eye failure in gigacycle fatigue", *Fatigue & Fracture of Engineering Materials & Structures*, vol. 22, no. 7, pp. 601–607, 1999.

[OTS 80] OTSUKA A., MORI K., OSHIMA T. *et al*., "Mode II fatigue crack growth in aluminum alloys and mild steel", in FRANÇOIS D. (ed.), *Advances in Fracture Research*, Pergamon Press, 1980.

[PAP 94] PAPADOPOULOS I.V., "A new criterion of fatigue strength four out-of-phase bending and torsion of hard metals", *Int. J. Fatigue*, vol. 16, pp. 377–384, 1994.

[PAP 97] PAPADOPOULOS I.V., DAVOLI P., GORLA C. *et al*., "A comparative study of multiaxial high-cycle fatigue criteria for metals", *Int. J. Fatigue*, vol. 19, no. 3, pp. 219–235, 1997.

[PAR 63] PARIS P.C., ERDOGAN F., "A critical analysis of crack propagation laws", *Trans. ASME, J. Bas. Eng*., vol. 85, pp. 528–534, 1963.

[PEA 75] PEARSON S., "Initiation of fatigue cracks in commercial aluminum alloys and the subsequent propagation of very short cracks", *Engineering Fracture Mechanics*, vol. 7, pp. 235–247, 1975.

[PED 90] PEDERSEN O.B., "Overview no. 89 – Mechanism maps for cyclic plasticity and fatigue of single phase materials", *Acta Metallurgica et Materialia*, vol. 38, no. 7, pp. 1221–1239, 1990.

[PEL 70] PELLOUX R.M.N., "Crack extension by alternate shear", *Engineering Fracture Mechanics*, vol. 1, pp. 697–704, 1970.

[PER 14] PERALTA P., LAIRD C., "Fatigue of metals", in LAUGHLIN D.E., HONO K. (eds), *Physical Metallurgy*, 5th ed., Elsevier, 2014.

[PES 11] PESSARD E., MOREL F., MOREL A. *et al*., "Modelling the role of non-metallic inclusions on the anisotropic fatigue behaviour of forged steel", *Int. J. Fatigue*, vol. 33, no. 4, pp. 568–577, 2011.

[PET 91] PETIT J., HÉNAFF G., "Stage II intrinsic fatigue crack propagation", *Scripta Metallurgica et Materialia*, vol. 25, pp. 2683–2687, 1991.

[PET 92] PETIT J., KOSCHE K., GUDLADT H.J., "Intrinsic stage I crack propagation in Al-Zn-Mg single crystals", *Scripta Metallurgica et materialia*, vol. 26, pp. 1049–1054, 1992.

[PET 00] PETIT J., HÉNAFF G., SARRAZIN-BAUDOUX C., "Mechanisms and modeling of near-threshold fatigue crack propagation", in NEWMAN J.C., PIASCIK R.S. (eds), *Fatigue Crack Growth Thresholds Endurance Limits And Design*, ASTM STP, vol. 1372, 2000.

[PET 03] PETIT J., HÉNAFF G., SARRAZIN-BAUDOUX C., "Environmentally-assisted fatigue in the gaseous atmosphere", in PETIT J., SCOTT P. (eds), *Comprehensive Structural Integrity: Environmentally-Assisted Fracture*, vol. 6, Elsevier, 2003.

[PIP 91] PIPPAN R., "Threshold and effective threshold of fatigue crack propagation in Armco iron I. The influence of grain size and cold working", *Material Science and Engineering*, vol. A138, pp. 1–13, 1991.

[POM 02] POMMIER S., "Plane strain crack closure and cyclic hardening", *Engineering Fracture Mechanics*, vol. 69, pp. 25–44, 2002.

[POM 05] POMMIER S., RISBET M., "Time derivative equations for mode I fatigue crack growth in metals", *International Journal of Fatigue*, vol. 27, pp. 1297–1306, 2005.

[REI 98] REINHARD P., RIEMELMOSER F.O., "Visualization of the plasticity-induced crack closure under plane strain conditions", *Engineering Fracture Mechanics*, vol. 60, pp. 315–322, 1998.

[ROV 91] ROVEN H.J., NES E., "Cyclic deformation of ferritic steel – II. Stage II crack propagation (overview no. 94)", *Acta Metallurgica Materialia*, vol. 39, pp. 1735–1754, 1991.

[SAN 13] SANGID M.D., "The physics of fatigue crack initiation", *Int. J. Fatigue*, vol. 57, pp. 58–72, 2013.

[SAX 78] SAXENA A., HUDAK S.J., "Review and extension of compliance information for common crack growth specimens", *Int. J. Fracture*, vol. 14, pp. 453–468, 1978.

[SMI 88] SMITH M.C., SMITH R.A., "Toward an understanding of mode II fatigue crack growth", in FONG J.T., WEI R.P., FIELDS R.J. *et al.* (eds), *Basic Questions in Fatigue I*, ASTM STP, vol. 924, Philadelphia, 1988.

[STA 89] STANZL S., CZEGLEY M., MAYER H.R. *et al*., "Fatigue crack growth under combined mode I and mode II loading", in WEI R.P., GANGLOFF R.P. (eds), *Fracture Mechanics: Perspectives and Directions*, ASTM STP, vol. 1020, Philadelphia, 1989.

[STO 78] STOLTZ R.E., PINEAU A.G., "Dislocation-precipitate interaction and cyclic stress-strain behavior of a γ′ strengthened superalloy", *Materials Science and Engineering*, vol. 34, no. 3, pp. 275–284, 1978.

[SUR 81] SURESH S., ZAMISKI Z.A., RITCHIE R.O., "Oxide-induced crack closure: An explanation for near-threshold fatigue crack growth behavior", *Metallurgical Transactions A*, vol. 12A, pp. 1435–1443, 1981.

[SUR 82] SURESH S., RITCHIE R.O., "A geometric model for fatigue crack closure induced by fracture surface morphology", *Metallurgical Transactions A – Physical Metallurgy and Materials Science*, vol. 13A, pp. 1627–1631, 1982.

[SUR 83] SURESH S., RITCHIE R.O., "Near-threshold fatigue crack propagation: A perspective on the role of crack closure", in DAVIDSON D.L., SURESH S. (eds), *Fatigue Crack Growth Thresholds Concepts*, 1983.

[SUR 84] SURESH S., VASUDEVAN A.K., BRETZ P.E., "Mechanisms of slow fatigue crack-growth in high-strength aluminum-alloys – role of microstructure and environment", *Metallurgical Transactions A*, vol. 15, pp. 369–379, 1984.

[SUR 98] SURESH S., *Fatigue of Materials*, Cambridge University Press, Cambridge, 1998.

[TSC 88] TSCHEGG E.K., STANZL S.E., "The significance of sliding mode crack closure on mode IIIfatigue crack growth", in FONG J.T., WEI R.P., FIELDS R.J. *et al.* (eds), *Basic Questions in Fatigue 1*, ASTM STP, vol. 924, 1988.

[VOG 80] VOGELESANG L.B., SCHIJVE J., "Environmental effects on fatigue fracture mode transitions observed in aluminium alloys", *Fatigue & Fracture of Engineering Materials & Structures*, vol. 3, pp. 85–98, 1980.

[VOR 13a] VOR K., GARDIN C., SARRAZIN-BAUDOUX C. *et al*., "Wake length and loading history effects on crack closure of through-thickness long and short cracks in 304l: Part I – experiments", *Engineering Fracture Mechanics*, vol. 99, 266–277, 2013.

[VOR 13b] VOR K., GARDIN C., SARRAZIN-BAUDOUX C. *et al*., "Wake length and loading history effects on crack closure of through-thickness long and short cracks in 304l: Part II–3D numerical simulation", *Engineering Fracture Mechanics*, vol. 99, pp. 306–323, 2013.